Interfacial engineering design induces enriched-defects expediting the catalytic conversion kinetics of polysulfides

Guixin Zhang, Xiaorong Chen, Xinmeng Yu, Qingyu Li, Hongqiang Wang, Sijiang Hu, Juantao Jiang, Youguo Huang*, Zhaoling Ma*

Guangxi Key Laboratory of Low Carbon Energy Materials, Guangxi New Energy Ship Battery Engineering Technology Research Center, Guangxi scientific and technological achievements transformation pilot research base of electrochemical energy materials and devices, School of Chemistry and Pharmaceutical Sciences, Guangxi Normal University, Guilin 541004, China

E-mail: zhaolingma@163.com (Zhaoling Ma), huangyg72@163.com (Youguo Huang)

1. Experimental section

1.1. Materials preparation

1.1.1 Chemicals

Polyvinylpyrrolidone [PVP K30] (AR, Sinopharm Chemical Reagent Co., Ltd.), hydroxylated multi-walled carbon nanotubes [CNT] (Chengdu Organic Chemicals Co., Ltd.), Cobalt chloride hexahydrate [$CoCl_2 \cdot 6H_2O$] (AR, Xilong Chemical Co., Ltd.), Sodium molybdate dihydrate [$Na_2MoO_4 \cdot 2H_2O$] (AR, Xilong Chemical Co., Ltd.), Sublimed sulfur [S] (AR, Sinopharm Chemical Reagent Co., Ltd.), Lithium sulfide [Li_2S] (AR, Aladdin Co., Ltd.), Urea [$CO(NH_2)_2$] (AR, Xilong Chemical Co., Ltd.), Hydrochloric acid [HCl] (AR, Xilong Chemical Co., Ltd.).

1.1.2 Synthesis of Co-Mo/CNT precursors

Co-Mo/CNT precursors are prepared by a simple hydrothermal method. Firstly, 25 mg of surfactant polyvinylpyrrolidone (PVP, K30) is dissolved in 60 mL deionized water, and stirred until completely dissolved. Then 50 mg hydroxylated carbon nanotubes (CNT) are added, stirred and ultrasonic dispersed until even. The aqueous solution containing 10 mL 0.43 mmol $CoCl_2 \cdot 6H_2O$ and the aqueous solution containing 10 mL 0.43 mmol $Na_2MoO_4 \cdot 2H_2O$ are slowly dripped into the water and stirred for 30 min. Hydroxylated CNT can adsorb metal cations by electrostatic action to promote its in situ nucleation growth. The mixed liquid is put into the inner liner of a Teflon lined reactor and hydrothermal reaction at 150 ℃ in a blast drying oven for 6 h. After cooling, the mixture is vacuum-filtered, and the black solid products are wished with deionized water for 3 times. Finally, the products are collected overnight in a vacuum freeze-dryer. For comparison, the precursor with different Co-Mo precursors loads is prepared by regulating the concentrations of $CoCl_2 \cdot 6H_2O$ and $Na_2MoO_4 \cdot 2H_2O$. The molar ratio of cobalt source and molybdenum source is 1:1, and other conditions remained unchanged.

1.1.3 Synthesis of CoS_2-MoS_2/CNT composites

CoS_2-MoS_2/CNT composites are processed by a simple vapor phase annealing vulcanization method. The Co-Mo/CNT precursor prepared in the previous step is weighed at 100 mg and placed in

the middle of the quartz tube of the tubular furnace. Another 1000 mg of sublimated sulfur (S) is placed in another sintering boat and placed on the upstream of the quartz tube of the tubular furnace. In the atmosphere of argon, the room temperature is heated from 5 ℃/min to 450 ℃ for 4 h. Collect solid samples after cooling, seal, and dry storage. For comparison, the CoS_2-MoS_2/CNT composites with different metal sulfide loads (n= 10%, 20%, 30% (prepared from 0.43 mmol cobalt and molybdenum sources) and 40%). CoS_2-MoS_2/CNT composites are prepared by vulcanizing the precursor with different Co-Mo compound loads in the previous process. Other conditions remained unchanged.

1.1.4 Synthesis of CoS_2/CNT composites

CoS_2/CNT composites are also prepared by simple hydrothermal and annealed vulcanization methods in order to control the synthesis of the same conditions. First, 25 mg of surfactant polyethylpyrrolidone (PVP, K30) is dissolved in 60 mL deionized water, and magnetic stirring is performed for 10 min until PVP is completely dissolved. Then 50 mg hydroxylated multi-walled carbon nanotubes (MWCNT) are added, stirred for 10 min and placed in an ultrasonic cleaner for ultrasonic dispersion for 1 h. Then 0.34 mmol $CoCl_2 \cdot 6H_2O$ and 1.38 mmol urea ($CO(NH_2)_2$) are added to stir for 30 min, followed by hydrothermal reaction in 150 ℃ for 6 h. After cooling, vacuum filtration is carried out, and the black solid products are wished with deionized water and ethanol for 3 times. Finally, they are put in the vacuum freeze dryer overnight. Collected product $Co(OH)_2$/CNT. The $Co(OH)_2$/CNT precursor is cured by annealing at 450 ℃ in a tubular furnace for 4 h to obtain CoS2/CNT, and the metal sulfide load is controlled to 30%.

1.1.5 Synthesis of MoS_2/CNT composites

In order to control the synthesis of the same conditions, MoS_2/CNT composites are also prepared by simple hydrothermal method and annealing vulcanization method. First, 25 mg of surfactant polyethylpyrrolidone (PVP, K30) is dissolved in 60 mL deionized water, and magnetic stirring is performed for 10 min until PVP is completely dissolved. Then 50 mg hydroxylated multi-walled carbon nanotubes (MWCNT) are added, stirred for 10 min and placed in an ultrasonic cleaner for ultrasonic dispersion for 1 h. Then 0.22 mmol $Na_2MoO_4 \cdot 2H_2O$ and 0.308 mmol glucose ($C_6H_6O_6$, reducing agent) are added into the mixture for 15 min, and 0.6 mL 10 M concentrated hydrochloric acid (HCl) is added into the mixture drop by drop. The mixture is then subjected to hydrothermal reaction in 180 ℃ for 12 h in a blast oven. After cooling, vacuum filtration is performed, and the black solid products are wished with deionized water and ethanol for 3 times. Then, the black solid products MoO_2/CNT are collected by freeze-drying. The MoO_2/CNT precursor is cured by annealing at 450 ℃ in a tube furnace for 4 h to obtain MoS_2/CNT, and the metal sulfide load is controlled to 30%.

1.1.6 Preparation of Li_2S_6 solution and Visual adsorption experiment

To prepare 0.2 M Li_2S_6 solution, the sublimed sulfur and lithium sulfide with a molar ratio of 5:1

were added into the mixed solvent of 1, 2-dimethoxyethane/1, 3-dioxolane (DME/DOL, v:v=1:1) and stirred at 60 ℃ for 12 h until formed a homogeneous solution. Then, 10 mg powder samples (CNT, CoS_2/CNT, MoS_2/CNT, CoS_2-MoS_2/CNT) were immersed into the vials with 4 mL of diluted 2 mM Li_2S_6 solution, respectively. These vials were gentle shaken by hand for several times to disperse the samples, and digital image was recorded after 12 h of absorption. All of the above operations were carried out in an argon-filled glove box. To more accurately estimate the absorption ability of samples for Lithium polysulfide, the UV-Vis spectra experiments were measured for the of the supernatant diluted 30 times after soaking the samples.

1.1.7 Assembly and tests of Li_2S_6 symmetric cells

To fabricate the electrodes, 80 wt% the powder samples (CNT, CoS_2/CNT, MoS_2/CNT, CoS_2-MoS_2/CNT), 10 wt% Super P and 10 wt% PVDF were added into a moderate NMP solvent to form the uniform slurries, following by coating onto Al foils and vacuum drying oven overnight at 60 ℃ for 12 h. The coating Al foils were punched into a 14 mm diameter round sheet as identical the work electrodes and counter electrodes. The electrodes were assembled into the CR2025 coin cells with a Celgard 2500 separators and 50 μL of 0.2 M Li_2S_6 electrolyte containing 1 M LiTFSI (25 μL for each side of the separator). As a contrast, the cells of electrolyte without Li_2S_6 were assembled based on the same method to eliminate the contribution of electrical double-layer capacitor. Cyclic voltammetry (CV) measurements of the symmetric cells were operated from -0.8 V to 0.8 V at a scan rate of 5 mV/s. Electrochemical impedance spectroscopy (EIS) was carried out in a sinusoidal voltage. The amplitude was identified to 5 mV and the frequency range was between 0.01 Hz and 100 kHz.

1.1.8 Li_2S nucleation tests

Li_2S_8 solution (0.2 M) was prepared by mixing S_8 and Li_2S (molar ratio of 7:1) in tetraglyme solvent containing 1M LITFSI under vigorous stirring at 50 °C until formed a well-distributed solution. Commercial carbon paper (CP) was used as the current collector to load samples (CNT, CoS_2/CNT, CoS_2/CNT and CoS_2-MoS_2/CNT) with a loading about 1.5 mg. The obtained electrode, Li foil and Celgard 2500 membrane were selected as the cathode, anode and separator. 25 μL of Li_2S_8 solution (0.2 M) was dropped onto the cathode side, and then 25 μL of LiTFSI (0.2 M) without Li_2S_8 solution was dispersed to the Li anode side to obtain the CR2032 coin cells. The assembled cells firstly were galvanostatically discharged to 2.06 V at 0.112 mA and then discharged potentiostatically at 2.05 V until the current dropped below 10^{-5} A to allow Li_2S nucleation. Faraday's law is used for the calculation of the Li_2S nucleation capacity of the integral area of plotted curves. The nucleation capacity of Li_2S is calculated by the integral area of the plotted curves based on Faraday's law. The earlier peak position (t_m) represents the quicker Li_2S nucleation and growth rate constant (Ak^2), which is based on the following **Eq. 1**.

$$Ak^2 = 2/\pi t_m^3 \quad \text{Eq. (1)}^1$$

1.1.9 Preparation of the functional separators

The powder samples (CNT, CoS_2/CNT, CoS_2/CNT and CoS_2-MoS_2/CNT), Super P and PVDF with a mass ratio of 8:1:1 were dispersed into NMP solvent to form the homogeneous slurries which was coated on PP separators (Celgard-2500), and then dried in a vacuum oven at 45 ℃ overnight. Finally, the dried functional separators were cut into round sheets with a diameter of 16.2 mm. The loading of catalysts on the functionalized separators is around 0.4 mg cm^{-1}.

1.1.10 Fabrication of S/rGO cathode and Li-S coin cells assembly

The S/rGO materials were synthesized by the typical melting diffusion method. Firstly, sublimed sulfur with the mass ratio of 9:1 was exhaustively mixed with rGO in a mortar until uniform. Then, the mixed material was heated in a tubular furnace at 155 ℃ for 12 h under argon atmosphere as well as was heated to 200℃ for 150 min to dislodge the sulfur on the surface of the material. TGA experiment analyzed the content of sulfur in the S/rGO. S/rGO, Super P and PVDF with a weight ratio of 8:1:1 were dispersed in suitable NMP solvent to produce the homogeneous slurries, following by coating onto Al foils and vacuum drying at 60 ℃ for 12 h. The coated Al foils were punched into a 12 mm diameter round sheets as cathodes, the sulfur loading was about 1.2-1.4 mg/cm^2, and E/S (electrolyte/sulfur) ratio is identified as 15 μL/mg for general Li-S cells. The S/rGO cathode was assembled into the CR2032 coin Li-S cells with the functional separators (CNT, CoS_2/CNT, CoS_2/CNT and CoS_2-MoS_2/CNT), as well as a certain amount of DOL/DME electrolyte composing of 1 M LiTFSI and 1 % $LiNO_3$ (E/S in coin cells was 15 μm/mg). All of steps of cell assemblies were proceeded in an argon-filled glovebox (H_2O:≤0.01 ppm, O_2:≤0.01 ppm). CV curves and EIS tests was measured on electrochemical station (Germany ZAHNER Elektrik). CV measurement were conducted between 1.7 V and 2.8 V at the scan rate of 0.1, 0.2, 0.3, 0.4 and 0.5 mV/s. Electrochemical impedance spectroscopy (EIS) was operated with an AC voltage amplitude of 5 mV at the open-circuit potential, and the frequency range was between 10 mHz and 100 kHz. The galvanostatic charged and discharged are conducted on the LAND CT2001A test system (Wuhan Landian Electronics Co., LTD) with a voltage window 1.7-2.8 V under different current densities (1C = 1675 mA/g).

1.1.11 Li^+ diffusion coefficient evaluation

The Li^+ diffusion coefficient (D_{Li^+}) of the Bare, CNT, CoS_2/CNT, MoS_2/CNT, and CoS_2-MoS_2/CNT separators is evaluated by the CV curves at various scan rates based on the classic Randles-Sevcik equation as follows from **Eq. 2**.

$$I_p = (2.69\times10^5)\, Av^{0.5}n^{1.5}D_{Li}{}^{+0.5}C_{Li}{}^{+} \quad \text{Eq. (2)}^2$$

Where I_p (A g^{-1}) represents the peak current densities, A (1.13 cm^2) stands for the area of the cathode, v (0.1-0.5 V s^{-1}) is the scan rates, n (n=2) means the electron transfer number, $C_{Li}{}^{+}$ (1.1 mol

cm^{-3}) indicates the Li^+ concentration in the electrolyte. The values of D_{Li^+} can be calculated by the slope (k) of the linear relationship of the peak current densities (I_p) versus the square root of the scan rate ($v^{0.5}$).

1.1.12 *In-situ* Raman spectroscopy experiments

Li-S coin cells with a quartz window on the negative shell are used for the *In-situ* Raman spectroscopy experiments. A hole of 4 mm is punched on the Li-metal anode to allow the laser of 785 nm to shine on separator, and the schematic diagram of *In-situ* device are presented in **Fig. S14**. The cells are operated at a rate of 0.2 C (1 C = 1675 mA/g) to discharge and charge.

1.2. Materials Characterization

The morphologies of the prepared materials are characterized by Scanning electron microscope (SEM, FEI Quanta 200 FEG) and Transmission electron microscopy (TEM, Thermo Fisher Scientific Talos F200S). Crystal structures of the prepared materials are analyzed by X-ray diffraction (Rigaku D/max-2500) and Raman spectra in the wavelength of 785 nm (Renishaw in Via); chemical environment is studied by X-ray photoelectron spectroscopy (XPS, Thermo Fisher Scientific K-Alpha). The sulfur content in S/rGO materials is evaluated by Thermogravimetric Analysis (TGA, NETZSCH TG 209F1 Libra) under N_2 atmosphere, whose temperature from 30 ℃ to 600 ℃ at a temperature ramp rate of 10 ℃/min. The electron paramagnetic resonance (EPR) signals of the prepared materials are collected by an Endor spectrometer (Bruker A300) at room temperature.

2. Supporting Figures and Tables

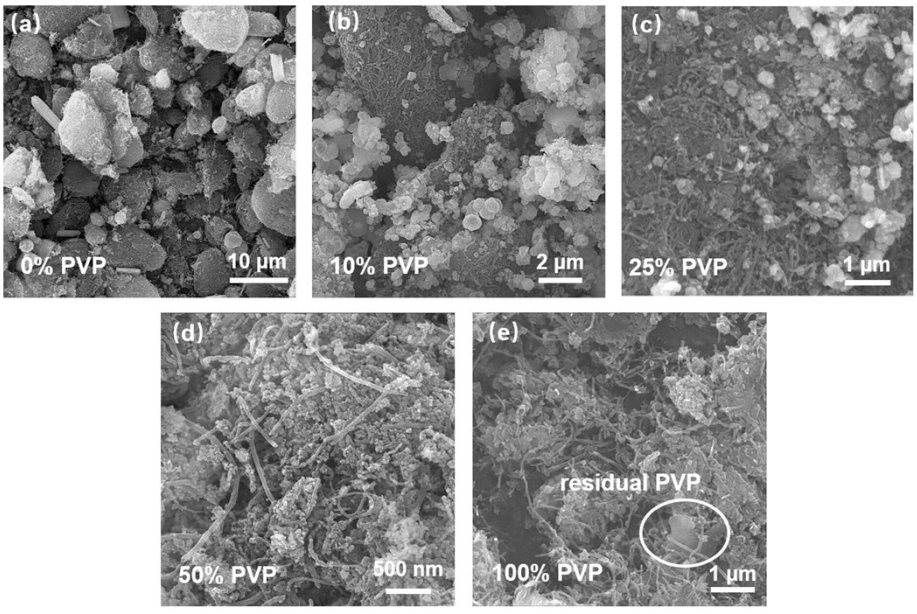

Figure S1. SEM images of $CoS_{2\text{-}MoS2}$/CNT-x, x is the mass ratio of PVP to CNT. (a) 0%, (b) 10%, (c) 25%, (d) 50%, and (e)100%.

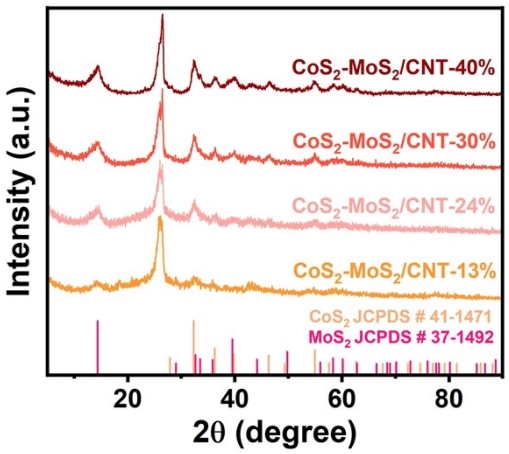

Figure S2. XRD patterns of CoS_2-MoS_2/CNT-n% with different metal composite contents for n= 16%, 24%, 30% and 40%.

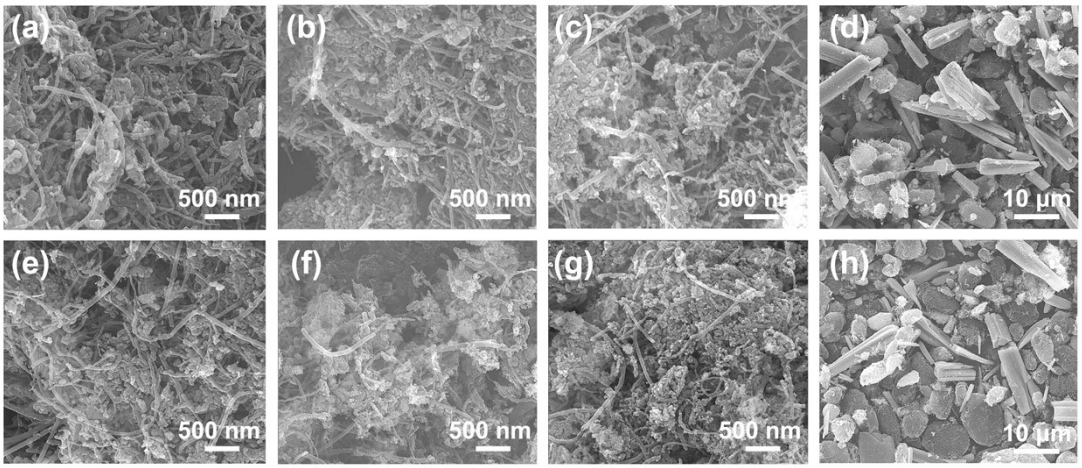

Figure S3. SEM images of Co-Mo/CNT-n% precursor and CoS_2-MoS_2/CNT-n% with different metal composite contents for n= 16%, 24%, 30% and 40%.

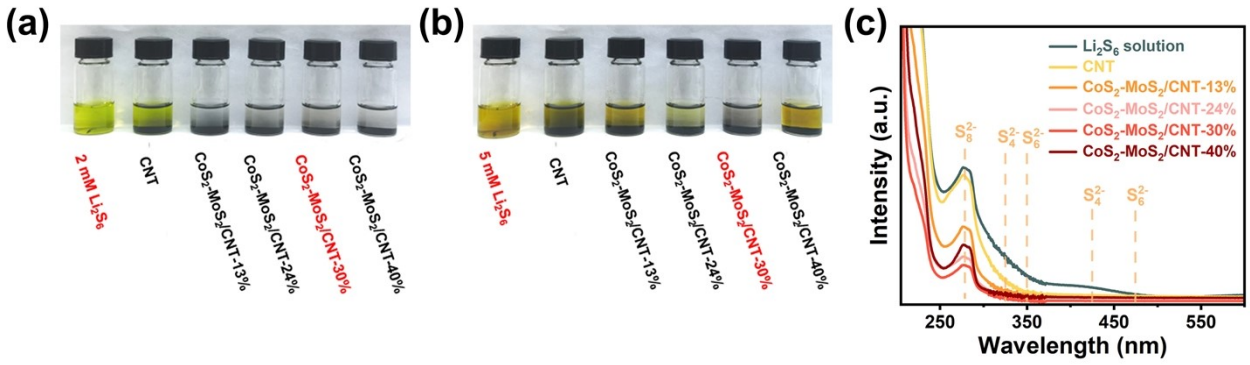

Figure S4. Digital photographs of 2 mM (a) and 5 mM (b) Li_2S_6 absorption experiment for CoS_2-MoS_2/CNT-n% with different metal composite contents for n= 16%, 24%, 30% and 40%. (c) UV-VIS spectrum of 5 mM Li_2S_6 solution after absorption.

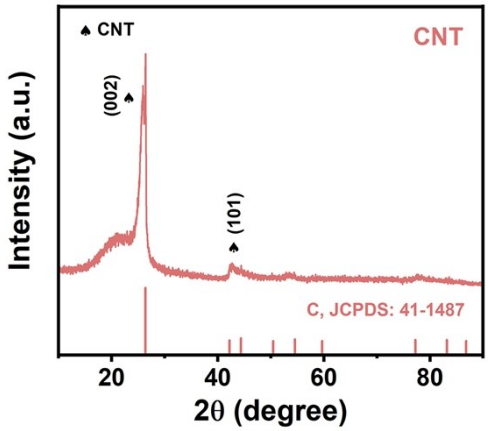

Figure S5. XRD patterns of CNT.

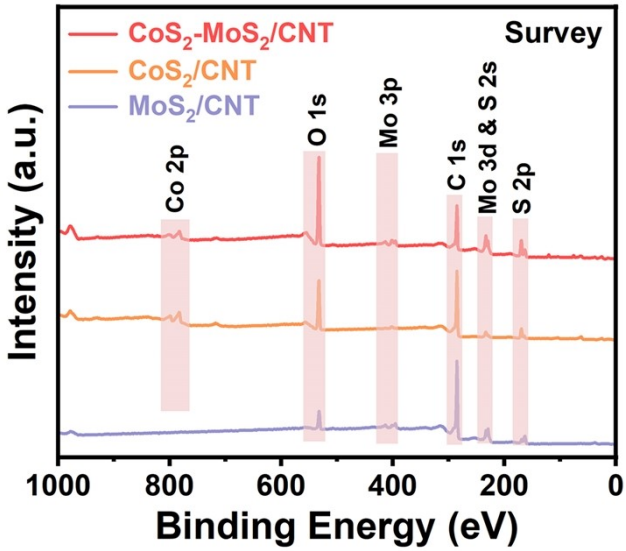

Figure S6. XPS survey spectrum of CoS_2/CNT, MoS_2/CNT and CoS_2-MoS_2/CNT.

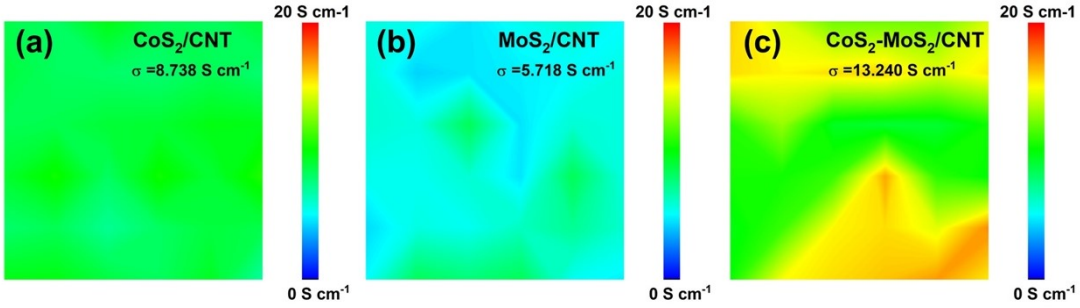

Figure S7. Average conductivity of (a) CoS_2/CNT, (b) MoS_2/CNT and (c) CoS_2-MoS_2/CNT.

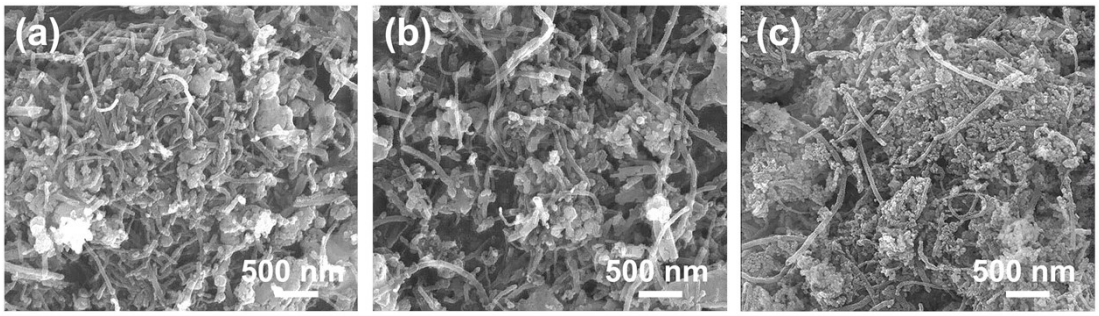

Figure S8. SEM images of (a) CoS_2/CNT, (b) MoS_2/CNT, (c) CoS_2-MoS_2/CNT.

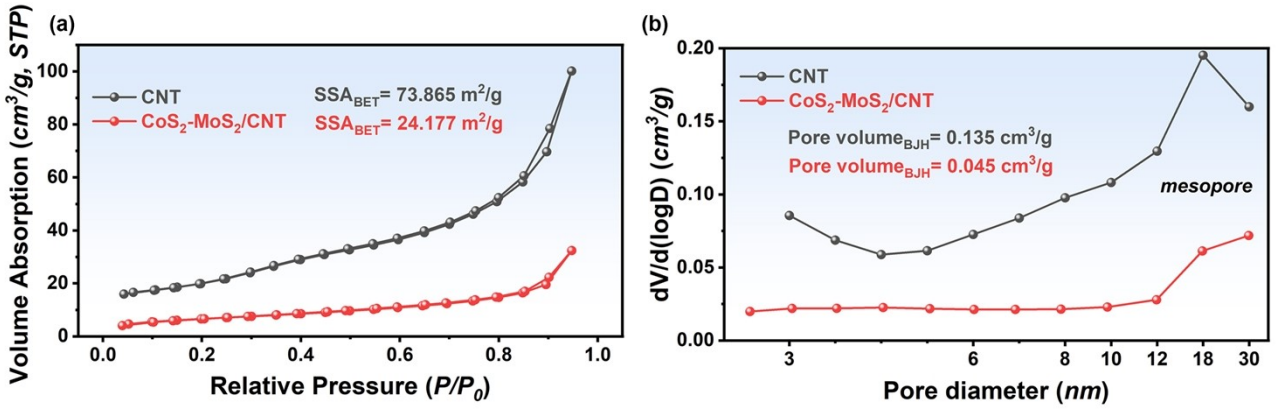

Figure S9. (a) N_2 adsorption-desorption isotherms, (b) corresponding pore diameter distributions of CoS_2-MoS_2/CNT and CNTs.

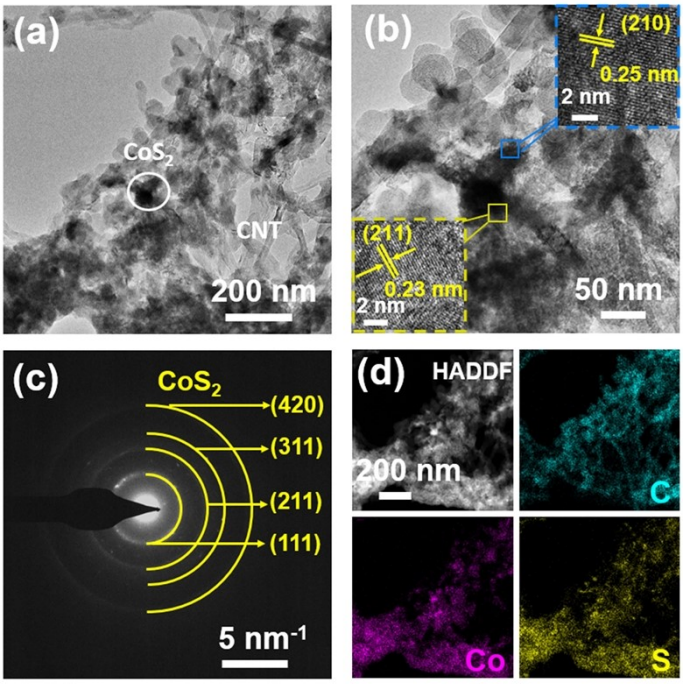

Figure S10. (a, b) TEM images (inset: HRTEM image). (c) SAED pattern (d) EDS mapping of CoS_2/CNT.

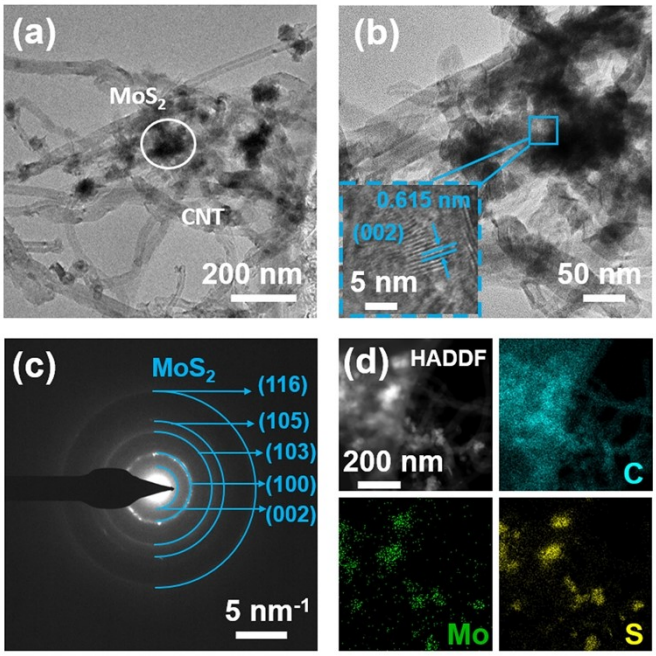

Figure S11. (a, b) TEM images (inset: HRTEM image). (c) SAED pattern (d) EDS mapping of MoS_2/CNT.

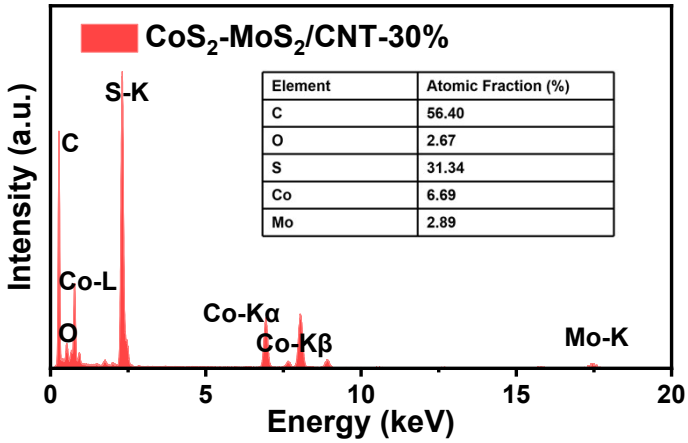

Figure S12. The EDS spectrum of CoS_2-MoS_2/CNT and its elemental analysis results.

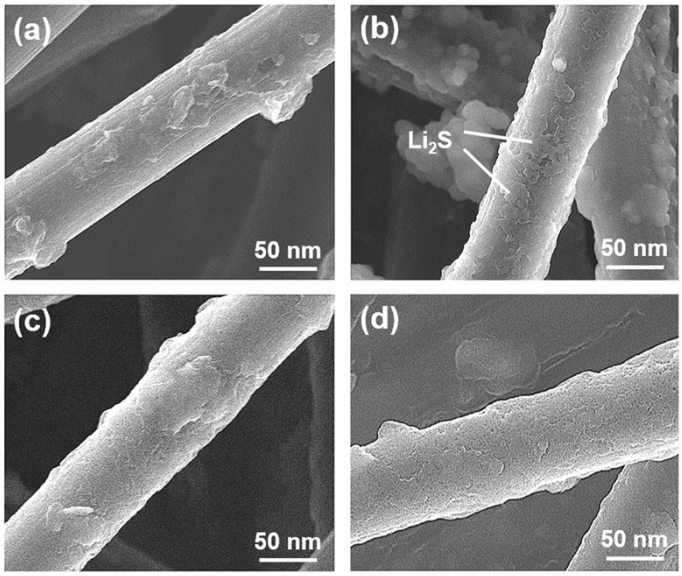

Figure S13. SEM images of (a) CP-CNT, (b) CP-CoS_2/CNT, (c) CP-MoS_2/CNT and (d) CP-CoS_2-MoS_2/CNT after Li_2S nucleation tests.

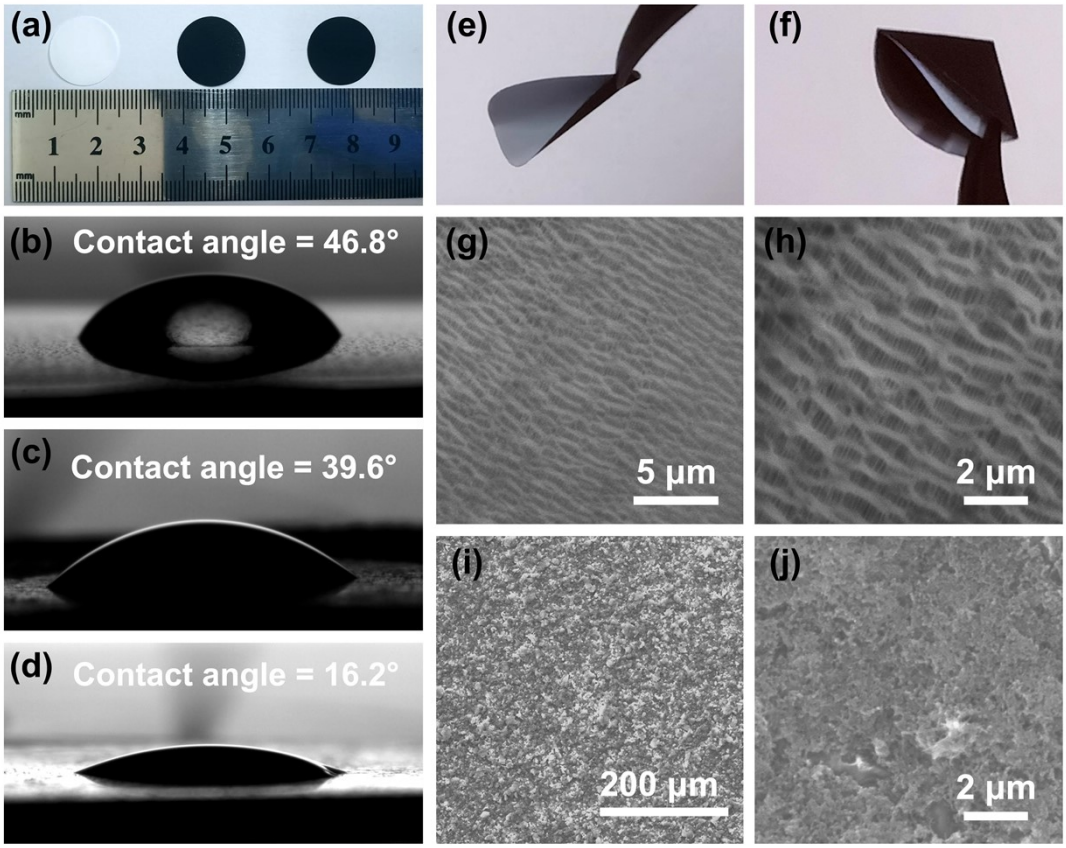

Figure S14. (a) Digital photograph of Bare, CNT and CoS_2-MoS_2/CNT separators are located left, center and right. Contact angle tests for (b) Bare, (c) CNT and (d) CoS_2-MoS_2/CNT separators. (e-f)

Bending and folding tests of CoS_2-MoS_2/CNT separator. SEM images for the surface of (g, h) Bare and (i, j) CoS_2-MoS_2/CNT separators.

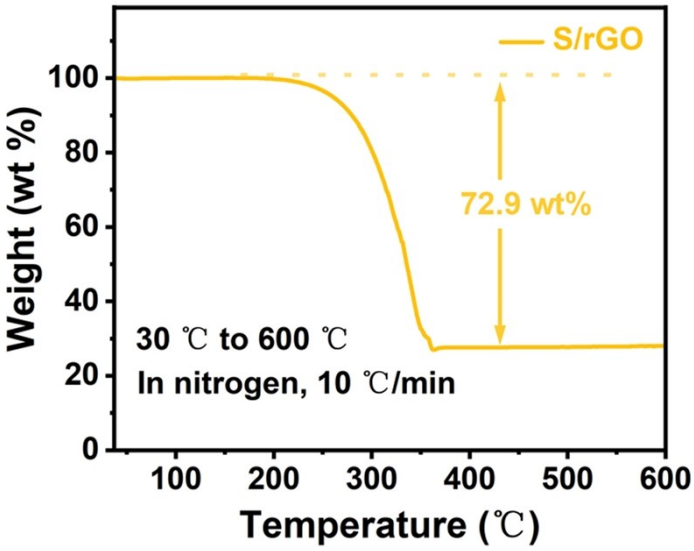

Figure S15. TGA curves of S/rGO.

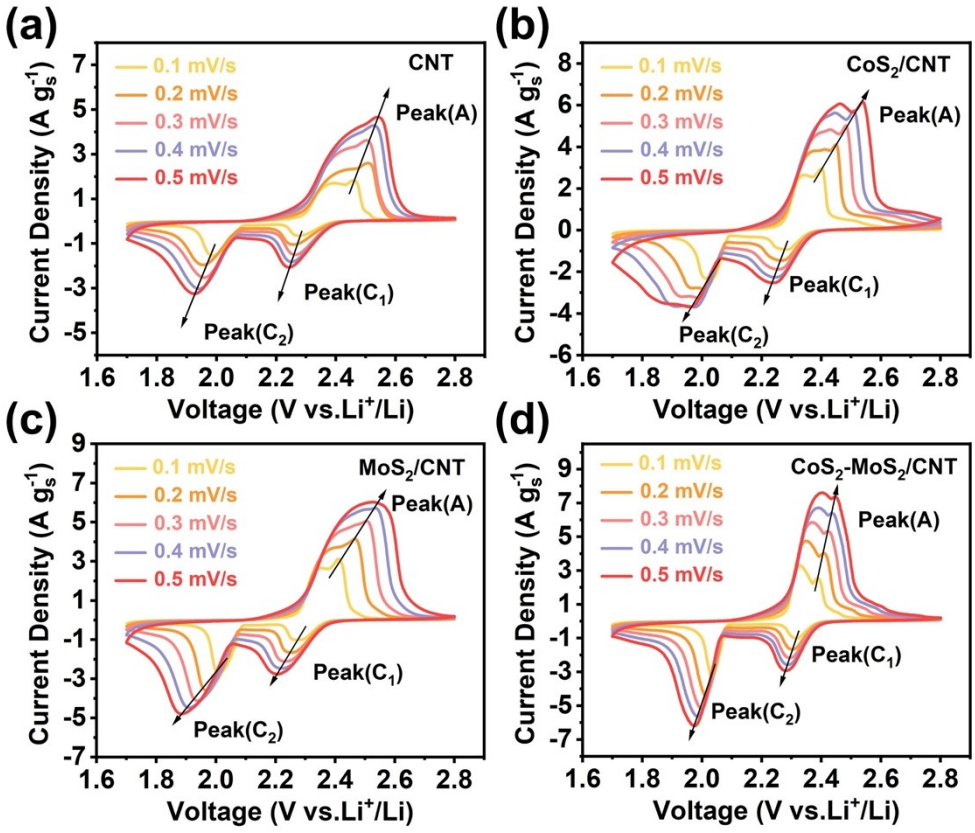

Figure S16. CV curves of Li-S cells with (a) CNT, (b) CoS_2/CNT, (c) MoS_2/CNT and (d) CoS_2-MoS_2/CNT separators at scan rates from 0.1-0.5 mV/s.

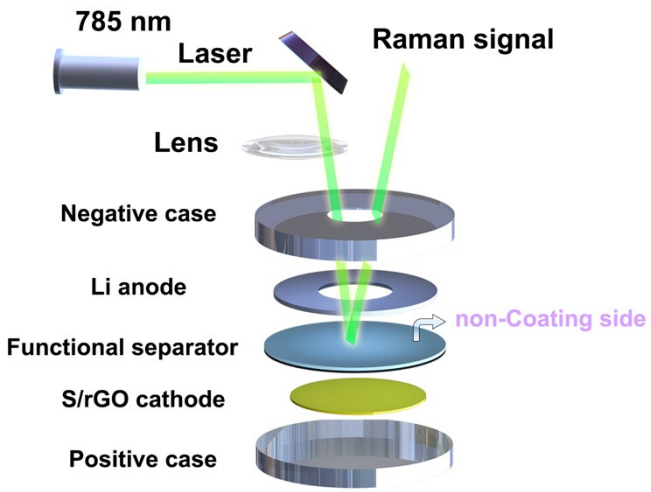

Figure S17. The schematic diagram of *In-situ* Raman device.

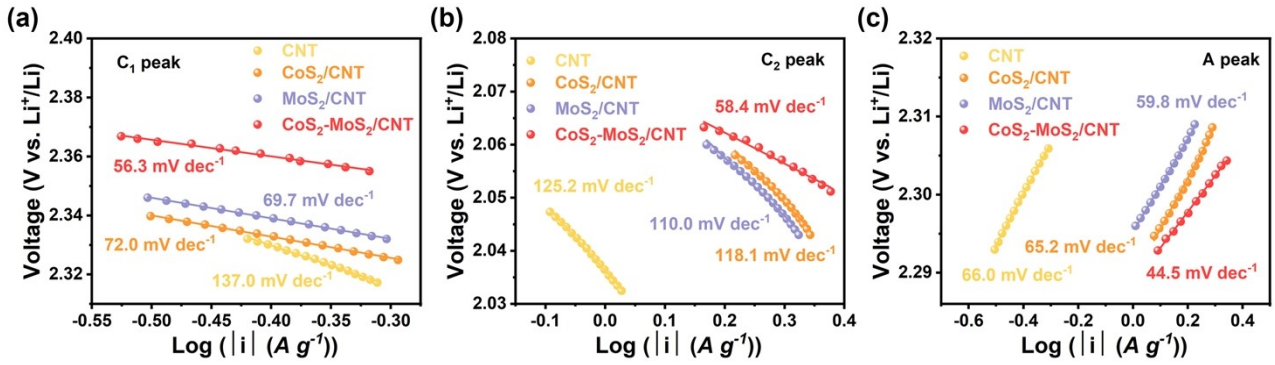

Figure S18. The Tafel slopes of the corresponding redox peaks (a) C_1, (b)C_2 and (c) A for different functionalized separators.

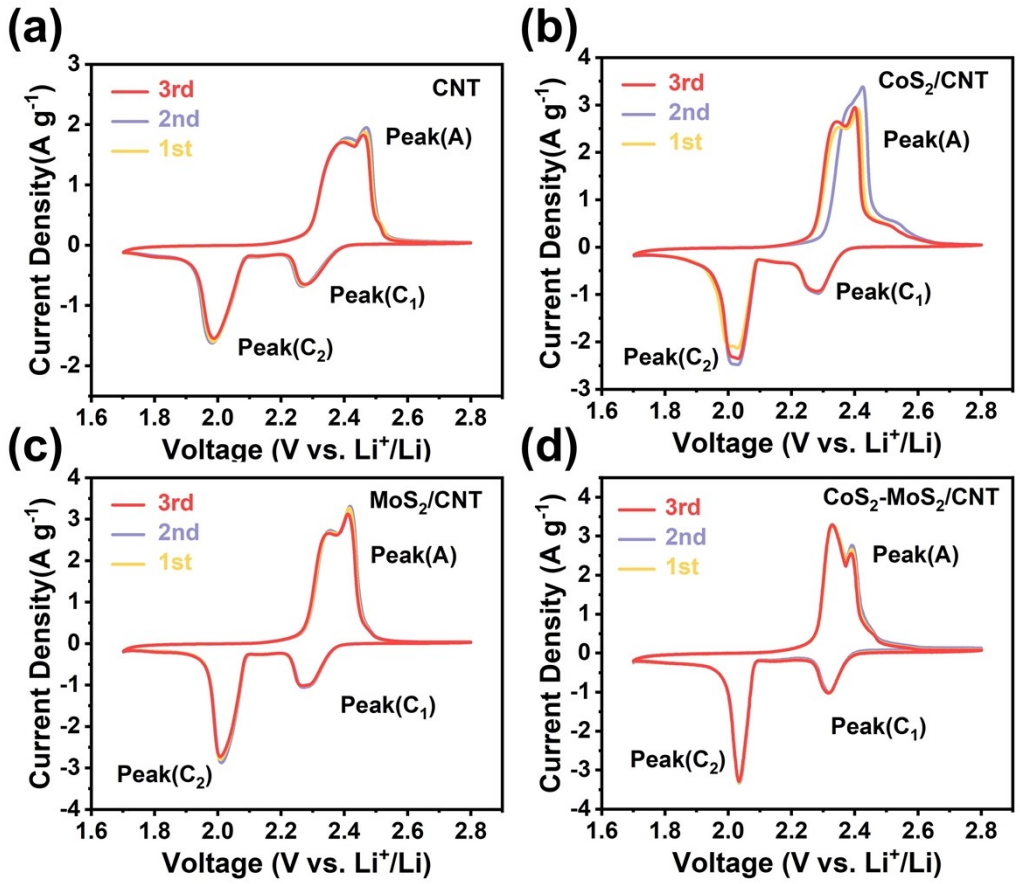

Figure S19. CV curves of the first three cycles of Li-S cells with (a) CNT, (b) CoS_2/CNT, (c) MoS_2/CNT and (d) CoS_2-MoS_2/CNT separators.

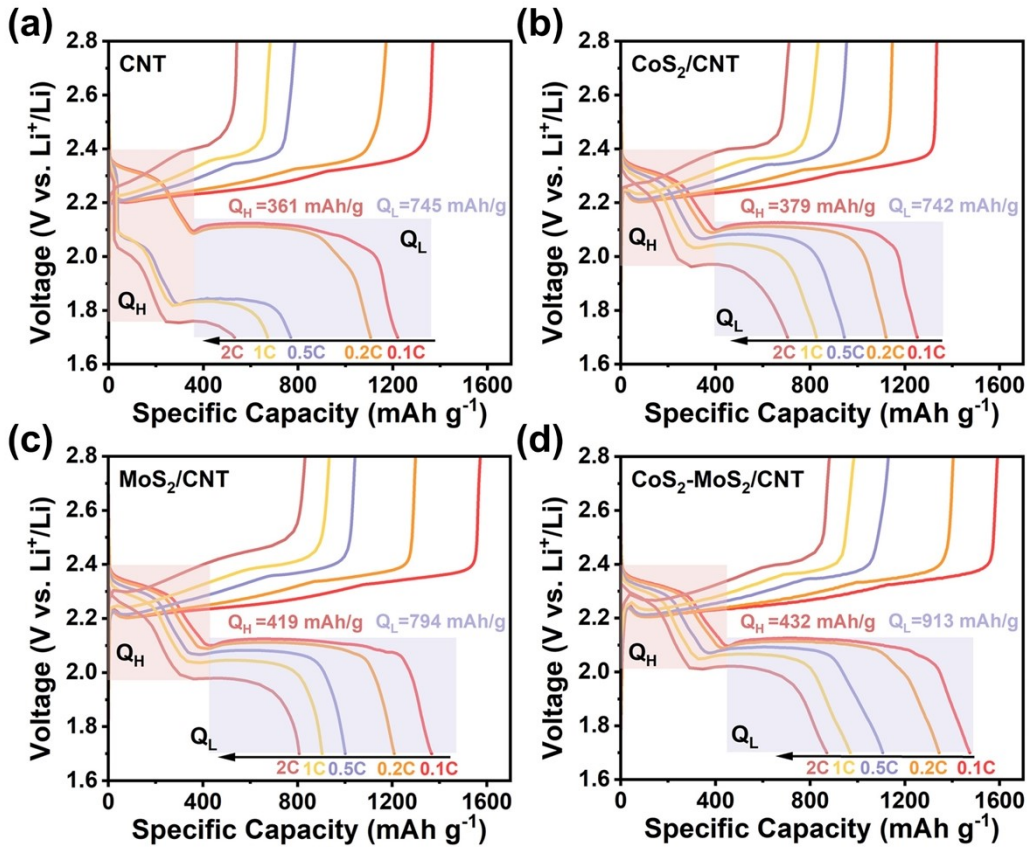

Figure S20. Galvanostatic charge-discharge profiles of Li-S cells based on different separators at 0.2-2C. (a) CNT, (b) CoS_2/CNT, (c) MoS_2/CNT and (d) CoS_2-MoS_2/CNT.

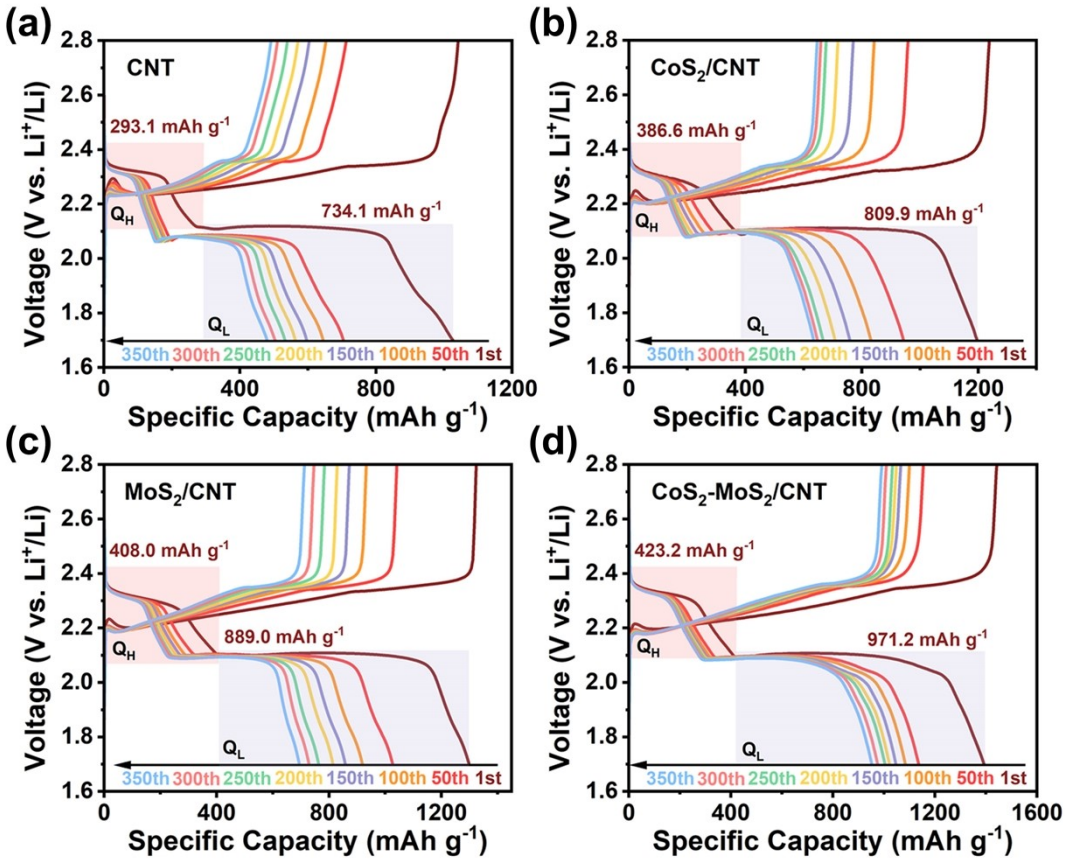

Figure S21. Galvanostatic charge-discharge profiles of Li-S cells based on different separators at various cycles. (a) CNT, (b) CoS_2/CNT, (c) MoS_2/CNT and (d) CoS_2-MoS_2/CNT. (The capacity contributed by the first and second discharge platforms is represented by Q_H and Q_L respectively).

Table S1. EIS fitting results of Li-S batteries with different separators before cycling.

Separator samples	R_s (Ω)	R_{ct} (Ω)
CNT	1.72	111.70
CoS_2/CNT	2.53	65.25
MoS_2/CNT	1.69	62.60
CoS_2-MoS_2/CNT	0.98	11.99

Table S2. EIS fitting results of Li-S batteries with different separators after 350 cycles.

Separator samples	R_s (Ω)	R_f (Ω)	R_{ct} (Ω)
CNT	5.33	10.92	7.69
CoS_2/CNT	2.81	8.93	8.56
MoS_2/CNT	4.20	10.66	3.34
CoS_2-MoS_2/CNT	2.70	5.30	1.96

Table S3. The comparison of rate performance for Li-S cells in this work and the literature (1 C = 1675 mA g^{-1}), and the corresponding plot is presented in Fig. 7c.

Catalysis materials	Rate performance (mAh g^{-1}) under various current density						Reference	Year
	0.1C	0.2C	0.5C	1C	2C	Switched back 0.2C		
CF/FeP@C	1250	1105	910	594	--	--	[3]	**2019**
PCCNT@ NPS	1161	983	854	795	655	1043.6	[4]	**2019**
rGO-CNT-CoP(A)	--	1157	962	906	821	959	[5]	**2020**
3DP-Ni_2P	--	973.8	843.2	743.1	637.6	923.8	[6]	**2021**
Ni/SiO_2/G	--	1080	882	826	782	1092	[7]	**2020**
CoO/CoP-Box	1248.1	1055.6	910.1	720.7	597.1	--	[8]	**2023**
Janus-S	1244	1080	862	692	583	--	[9]	**2021**
$CoNiO_2$/ Co_4N	--	1198	941	860	765		[10]	**2021**
β-$MoTe_2$/CNT	--	933	817	736	671	759	[11]	**2022**
PLG	1288	840	693.3	564.5	467.1	--	[12]	**2023**
CoS_2-MoS_2/CNT	--	1361.4	1111.2	969.3	869.4	1151.1	**This work**	**2023**

Table S4. The comparison of cycling performance for Li-S cells in this work and the literature.

Catalysis materials	Initial capacity (mAh g^{-1})	Current density (C)	Cycle number	Retention capacity (mAh g^{-1})	Capacity retention rate (%)	Decay ratio per cycle (%)	Reference	Year
FeP	1273.7	0.1	100	1038.4	81.5	0.185	[13]	**2018**
PCCNT@NPS	1118	0.2	100	958	85.7	0.143	[4]	**2019**
rGO-CNT-CoP(A)	1043.6	0.2	70	888.5	64	0.200	[5]	**2020**
NC/G	1380	0.2	100	980	71	0.290	[14]	**2019**
MC-NS	1172	0.2	100	907.5	77.4	0.225	[15]	**2019**
3DP-Ni_2P	942.8	0.2	50	775.9	82.3	0.354	[6]	**2021**
Ni/SiO_2/G	1282	0.2	100	831	64.8	0.280	[7]	**2020**
CoFe/ NHCS	1292	0.2	100	1023	79.2	0.208	[16]	**2021**
CoO/CoP-Box	1292.5	0.1	300	753.9	58.4	0.139	[8]	**2023**
PLG	1284.4	0.2	200	623.4	48.6	0.257	[12]	**2023**
HE-LSMO	1217.9	0.2	200	876.9	72	0.140	[17]	**2023**
CoS_2-MoS_2/CNT	1402.1	0.2	350	955.6	68.2	0.090	**This work**	**2023**
CF/FeP@C	695	1.0	200	500	71.9	0.14	[3]	**2019**
3DP-LaB_6/SP	835	2.0	1000	401	48	0.052	[18]	**2020**
TiN@C	883	1.0	600	636	72	0.05	[19]	**2021**
MnO_2	700	0.5	500	494	70.6	0.058	[20]	**2022**
CoP/C	938	1.0	500	562	59.9	0.08	[21]	**2019**
Janus-S	800	1.0	800	450	56.3	0.046	[9]	**2021**
Ni/NiO-C	793	1.0	500	484	61	0.078	[22]	**2022**
β-$MoTe_2$/CNT	873	1.0	300	585	67	0.11	[11]	**2022**
P-TiO_{2-x}	1049.8	1.0	600	508.1	48.4	0.086	[23]	**2022**

Fe_3C-FeN@NCF	895	1.0	800	393.8	44	0.07	[24]	**2023**
CoS_2-MoS_2/CNT	921.8	2.0	1000	589.1	63.9	0.036	**This work**	**2023**

3. Supporting References

1 M. Wang, L. Fan, X. Sun, B. Guan, B. Jiang, X. Wu, D. Tian, K. Sun, Y. Qiu, X. Yin, Y. Zhang and N. Zhang, *ACS Energy Lett.*, 2020, **5**, 3041-3050.

2 Y. Wang, Z. Deng, J. Huang, H. Li, Z. Li, X. Peng, Y. Tian, J. Lu, H. Tang, L. Chen and Z. Ye, *Energy Storage Mater.*, 2021, **36**, 466-477.

3 J. Shen, X. Xu, J. Liu, Z. Liu, F. Li, R. Hu, J. Liu, X. Hou, Y. Feng, Y. Yu and M. Zhu, *ACS Nano*, 2019, **13**, 8986-8996.

4 Z. Guang, Y. Huang, X. Chen, X. Sun, M. Wang, X. Feng, C. Chen and X. Liu, *Electrochim. Acta*, 2019, **307**, 260-268.

5 R. Sun, Y. Bai, M. Luo, M. Qu, Z. Wang, W. Sun and K. Sun, *ACS Nano*, 2020, **15**, 739-750.

6 F. Zhang, Z. Li, T. Cao, K. Qin, Q. Xu, H. Liu and Y. Xia, *ACS Sustainable Chem. Eng.*, 2021, **9**, 6097-6106.

7 C. Chen, Q. Jiang, H. Xu, Y. Zhang, B. Zhang, Z. Zhang, Z. Lin and S. Zhang, *Nano Energy*, 2020, **76**, 105033.

8 W. Zhou, X. Wang, J. Shan, L. Yue, D. Lu, L. Chen, J. Zhang and Y. Li, *J. Energy Chem.*, 2023, **80**, 128-139.

9 Y. Li, T. Gao, D. Ni, Y. Zhou, M. Yousaf, Z. Guo, J. Zhou, P. Zhou, Q. Wang and S. Guo, *Adv. Mater.*, 2021, **34**, 2107638.

10 J. Pu, W. Gong, Z. Shen, L. Wang, Y. Yao and G. Hong, *Adv. Sci.*, 2021, **9**, 2104375.

11 G. Lin, M. Liang, L. Liu, J. Liu, Z. Ao, Z. Shi and X. Ke, *ACS Appl. Mater. Interfaces*, 2022, **14**, 55616-55626.

12 C. Li, Q. Sun, Q. Zhang, C. Xu, S. Wang, Y. Ma, X. Shi, H. Zhang, D. Song and L. Zhang, *Chem. Eng. J.*, 2023, **455**, 140706.

13 S. Huang, Y. V. Lim, X. Zhang, Y. Wang, Y. Zheng, D. Kong, M. Ding, S. A. Yang and H. Y. Yang, *Nano Energy*, 2018, **51**, 340-348.

14 H. Xu, Q. Jiang, B. Zhang, C. Chen and Z. Lin, *Adv. Mater.*, 2019, **32**, 1906357.

15 J. Li, C. Chen, Y. Chen, Z. Li, W. Xie, X. Zhang, M. Shao and M. Wei, *Adv. Energy Mater.*, 2019,

9, 1901935.

16 Z. Gu, C. Cheng, T. Yan, G. Liu, J. Jiang, J. Mao, K. Dai, J. Li, J. Wu and L. Zhang, *Nano Energy*, 2021, **86**, 106111.

17 L. Tian, Z. Zhang, S. Liu, G. Li and X. Gao, *Nano Energy*, 2023, **106**, 108037.

18 J. Cai, Z. Fan, J. Jin, Z. Shi, S. Dou, J. Sun and Z. Liu, *Nano Energy*, 2020, **75**, 104970.

19 Y. Fan, K. Liu, A. Ali, X. Chen and P. K. Shen, *Electrochim. Acta*, 2021, **384**, 138187.

20 X. Wang, L. Yang, Y. Wang, Q. Li, C. Chen, B. Zhong, Y. Chen, X. Guo, Z. Wu, Y. Liu, Y. Liu and Y. Sun, *J. Colloid Interface Sci.*, 2022, **606**, 666-676.

21 J. Lin, K. Zhang, Z. Zhu, R. Zhang, N. Li and C. Zhao, *ACS Appl. Mater. Interfaces*, 2019, **12**, 2497-2504.

22 J. Pu, T. Wang, X. Zhu, Y. Tan, L. Gao, J. Chen, J. Huang and Z. Wang, *Electrochim. Acta*, 2022, **435**, 141396.

23 W. Zhang, Y. Xu, J. Liu, Y. Li, E. M. Akinoglu, Y. Zhu, Y. Zhang, X. Wang and Z. Chen, *Small Sci.*, 2022, **3**, 2200032.

24 M. Zhang, J. Mu, Y. Li, Y. Pan, Z. Dong, B. Chen, S. Guo, W. Yuan, H. Fang, H. Hu and M. Wu, *J. Energy Chem.*, 2023, **78**, 105-114.